JOURNAL OF MATERIALS SCIENCE **40** (2005) 4077–4084

Effects of nano-sized α_2(Ti_3Al) particles on quasi-static and dynamic deformation behavior of Ti-6Al-4V alloy with bimodal microstructure

DONG-GEUN LEE, SUNGHAK LEE
Center for Advanced Aerospace Materials, Pohang University of Science and Technology, Pohang, 790-784 Korea
E-mail: shlee@postech.ac.kr

A bimodal microstructure containing very fine α_2(Ti_3Al) particles was produced by over-aging a Ti-6Al-4V alloy. The effects of α_2 precipitation on quasi-static and dynamic deformation behavior were investigated in comparison with an unaged bimodal microstructure. Quasi-static and dynamic torsional tests were conducted on them using a torsional Kolsky bar. The quasi-static torsional test data indicated that the over-aged bimodal microstructure showed higher fracture shear strain than the unaged bimodal microstructure, while their maximum shear stresses were similar. Under dynamic torsional loading, both maximum shear stress and maximum shear strain of the over-aged microstructure were higher than those of the unaged microstructure. The possibility of the adiabatic shear band formation under dynamic loading was quantitatively analyzed by introducing concepts of critical shear strain, absorbed deformation energy, and void initiation. In the over-aged microstructure, the energy required for forming adiabatic shear bands was higher than that in the unaged microstructure, thereby lowering the possibility of the adiabatic shear band formation. The α_2 precipitation in the over-aged microstructure was effective in both the improvement of quasi-static and dynamic torsional properties and the reduction in the adiabatic shear banding, which suggested a new approach to improve ballistic performance of Ti alloy armor plates.

1. Introduction

Ti-6Al-4V alloy has high strength and stiffness as well as light weight [1–6], thereby providing a great potential for structural armor plates. Ballistic performance is known to correlate with dynamic deformation behavior as well as the formation of adiabatic shear bands [7], but only limited information is available on the dynamic deformation behavior of the Ti-6Al-4V alloy. An adiabatic shear band is a narrow region of highly localized plastic deformation [8, 9], and is often observed when materials are deformed at high strain rates such as ballistic impact, machining, and high-speed metal forming. It is also believed to initiate due to the development of a thermo-mechanical plastic instability. The localization generally induces a failure of structures through a loss of load-carrying capacity within the adiabatic shear band [8–10], and thus the adiabatic shear banding is of great interest to the ballistic performance of armor plates.

Recently, Lee *et al.* [11] investigated the possibility of the adiabatic shear band formation in three typical Ti-6Al-4V microstructures, i.e., Widmanstätten, equiaxed, and bimodal microstructures, by analyzing how deformation energy was distributed and consumed by either void initiation or adiabatic shear banding. Their results indicated that the bimodal microstructure could have excellent ballistic performance because the possibility of the adiabatic shear band formation was lowest of the three microstructures. However, studies on microstructures and heat treatment conditions, under which adiabatic shear banding is suppressed while excellent mechanical properties are promoted, are required. For example, when the Ti-6Al-4V alloy is over-aged at 500–600°C, nanometer-sized α_2 (Ti_3Al) phases can be homogeneously precipitated inside α phases, thereby leading to the additional improvement of mechanical properties [12–14]. Al in the Ti-6Al-4V alloy plays a role in increasing the α/β transformation temperature and in forming a region coexisting α and α_2 phases in the phase diagram because it works as an α stabilizing element [13]. α_2 phases are homogeneously precipitated in a form of very fine particles having a coherent relationship with α during aging. From this precipitation, the improvement of ballistic performance as well as general mechanical properties can be expected.

In this study, a bimodal microstructure containing fine α_2 particles was obtained by over-aging a Ti-6Al-4V alloy, and its quasi-static and dynamic deformation behavior was investigated in comparison to that of an unaged microstructure. Quasi-static and dynamic

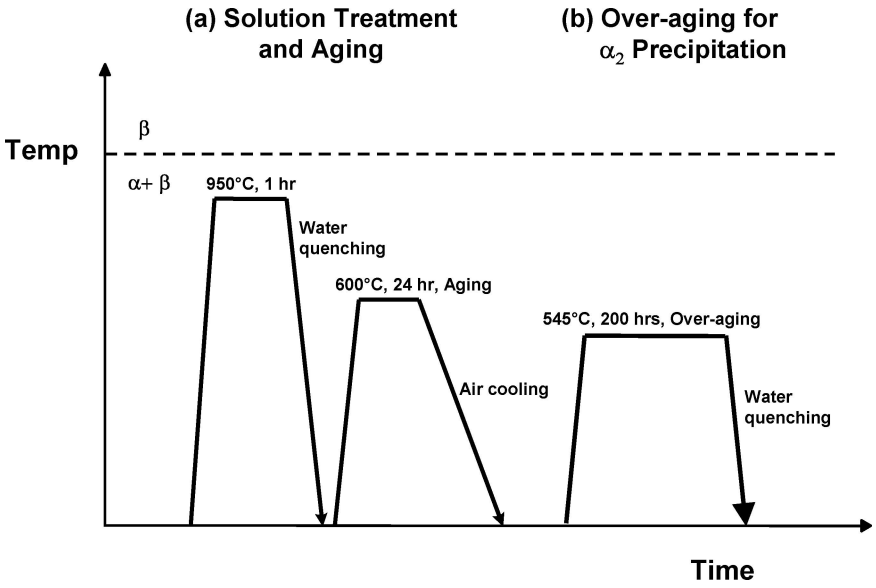

Figure 1 Schematic representation of heat treatments for (a) bimodal microstructure and (b) precipitation of fine α_2 particles.

torsional tests were conducted on them using a torsional Kolsky bar, and torsionally deformed areas beneath fracture surfaces were investigated to determine the deformation behavior and effects of α_2 precipitation.

2. Experimental

The material used in this study was a Ti-6Al-4V alloy plate (thickness; 50 mm) obtained from Supra Alloys Inc., U.S.A., and its chemical composition was 6.19Al-4.05V-0.19Fe-0.12O-0.02C-0.01N-0.004H-Ti (wt.%). This alloy plate was subjected to heat treatments as shown in Figs 1a and b to obtain a bimodal microstructure and to precipitate fine α_2 phases inside α phases [12, 14, 15]. The bimodal microstructure was obtained by holding at 950°C ($\alpha + \beta$ region) for 1 h, water quenching, and aging at 600°C for 24 h (Fig. 1a). It was then over-aged at 545°C for 200 h to precipitate α_2 phases (Fig. 1b).

Specimens were etched using a Kroll solution (H_2O 100 Mℓ , HF 3 Mℓ, HNO_3 5 Mℓ), and their microstructures were observed using an optical microscope and a scanning electron microscope (SEM). The size and volume fraction of each phase were measured using an image analyzer. Tensile bars with a gage length of 30 mm and a gage diameter of 6 mm were machined, and tensile tests were conducted at room temperature and at a strain rate of 10^{-3} sec^{-1}. Hardness of the microstructures aged at 545°C for 200–300 h were also measured using a Vickers hardness tester under a 2 kg load.

Thin-walled tubular specimens used for quasi-static and dynamic torsional tests had a gage length of 2.5 mm and a gage thickness of 280 μm. The torsional Kolsky bar consists of a pair of 2-meter long 2024-T6 aluminum bars with a diameter of 25.4 mm [16]. In the quasi-static torsional test, the incident bar is fixed by a clamp, and then the specimen is deformed slowly at a strain rate of about 10^{-4} sec^{-1} by transmitting power to the bar by a motor and two speed-reducing motors. Output voltage from the static bridge attached on the transmitter bar and those from two linear variable differential transformers are respectively recorded at an XYt-recorder and an oscilloscope. Each recorded data is transformed to shear stress and shear strain as a function of time, and the time term is eliminated to obtain a quasi-static shear stress-shear strain curve.

In the dynamic torsional test, a certain amount of torque is stored between a clamp and a dynamic loading pulley. When the clamp is fractured, at which time an elastic shear wave is momentarily transmitted to the specimen, the specimen is deformed. Incident wave, reflected wave, and transmitted wave are detected respectively at strain gages, and recorded at an oscilloscope. Among the recorded wave signals, average shear strain expressed as a function of time, $\gamma(t)$, is measured from the reflected wave, while shear stress, $\tau(t)$, from the transmitted wave. A dynamic shear stress-shear strain curve is obtained from these $\gamma(t)$ and $\tau(t)$ by eliminating the time term. Shear strain rate during the test was about 1750 sec^{-1}, and the test was done at room temperature. Detailed descriptions of the dynamic and quasi-static torsional testing are provided in references [16–18]. Fracture surfaces were observed using an SEM after the quasi-static and dynamic torsional tests.

3. Results

3.1. Microstructure

Figs 2a and b are optical and SEM micrographs of the over-aged bimodal microstructure. The over-aged bimodal microstructure consists of tempered martensite and equiaxed α, together with a small amount of residual β, as shown in Fig. 2a. α grain size was measured to be 19 μm, and volume fractions of tempered martensite, α, and β were measured to be 52, 39 and 9%, respectively. This microstructure is similar to the unaged one. Table I shows the quantitative analysis data of the microstructural factors of the unaged and over-aged microstructures. Since these factors are within the error range, the over-aging treatment hardly affects the optical microstructures. However, there are some differences in the high-magnification SEM micrograph of the over-aged bimodal microstructure as shown in Fig. 2b.

TABLE I Quantitative analysis results of the unaged and over-aged bimodal microstructures of the Ti-6Al-4V alloy

Microstructure	Parameter	Unaged	Over-aged
Bimodal	Primary α grain size (μm)	19	19
	Primary α volume fraction (%)	38	39
	Tempered Martensite volume fraction (%)	52	52
	β volume fraction (%)	10	9

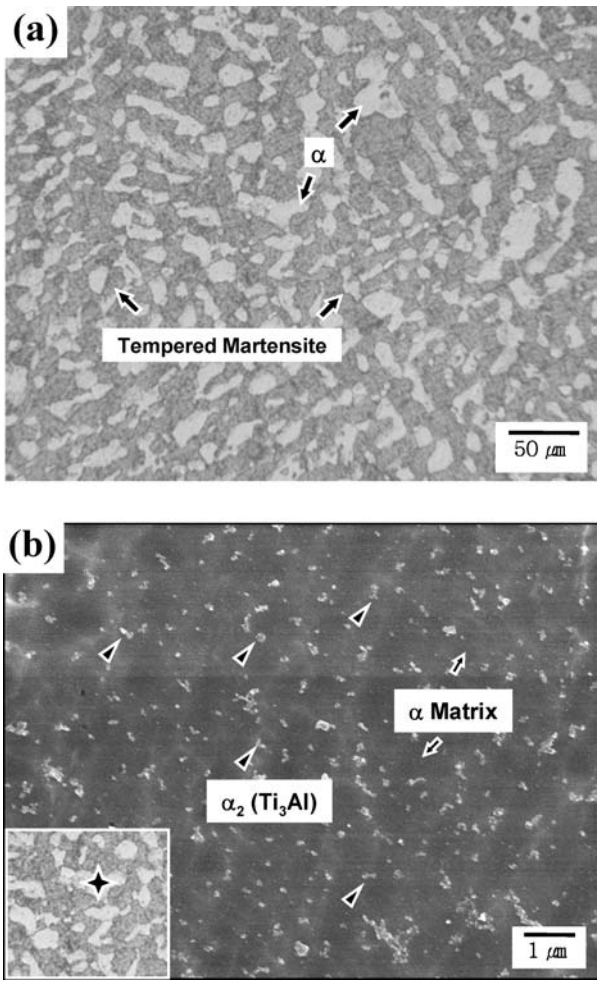

Figure 2 (a) Optical and (b) SEM micrographs of the over-aged bimodal microstructure. Very fine α_2 particles are homogeneously distributed in α phases as shown in (b). Kroll etched.

Fine α_2 phases of 50–200 nm in size are homogeneously distributed in the α phase. This matches well with the results of Welsch *et al.* [12] and Margolin *et al.* [13, 14].

3.2. Hardness and tensile properties

Fig. 3 shows the variation of Vickers hardness as a function of aging time at 545°C. The hardness tends to slightly increase with increasing the aging time, but the increase is not large.

The tensile test results of the bimodal microstructure before and after over-aging at 545°C for 200 h are listed in Table II. The unaged microstructure shows excellent yield strength, tensile strength, and elongation of 1070 MPa, 1134 MPa, and 10.7%, respectively. Yield and tensile strengths of the over-aged microstructure are lower than those of the unaged microstructure, while elongation is higher. This might be because the softening effect of martensite due to over-aging overrides the hardening effect due to α_2 precipitation.

TABLE II Room-temperature tensile results of the unaged and over-aged bimodal microstructures of the Ti-6Al-4V alloy

Microstructure	Yield strength (MPa)	Ultimate tensile strength (MPa)	Elongation (%)
Unaged bimodal	1070	1134	10.7
Over-aged bimodal	1033	1068	12.6

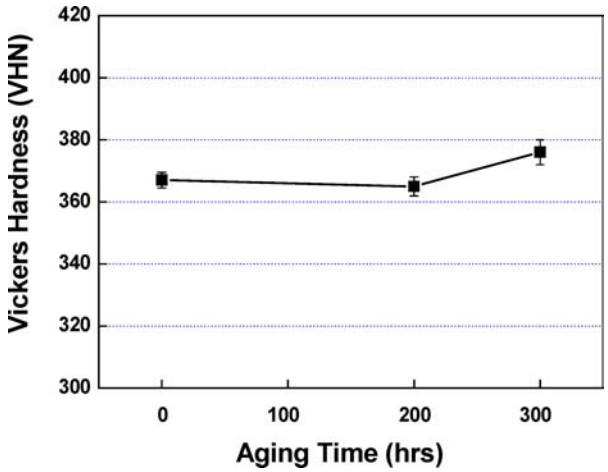

Figure 3 Variation of Vickers hardness as a function of aging time.

Figs 4a and b are SEM fractographs of the tensile specimens, and show a typical ductile fracture mode composed of dimples. In the unaged microstructure, large and small dimples are mixed, because interfaces between α and tempered martensite generate large voids whereas those between martensite platelets generate small voids (Fig. 4a) [11]. Dimple size of the over-aged microstructure is slightly smaller than that of the unaged microstructure (Fig. 4b).

3.3. Quasi-static torsional properties

Fig. 5 presents shear stress-shear strain curves obtained from the quasi-static torsional test. From these curves, maximum shear stress, shear strain at maximum shear stress point, and fracture shear strain were measured, and are summarized in Table III. Maximum shear stresses measured before and after over-aging are similar, and roughly satisfy the relationship of $\sigma = \sqrt{3}\tau$,

TABLE III Quasi-static and dynamic torsional properties of the unaged and over-aged bimodal microstructures of the Ti-6Al-4V alloy

Loading condition	Microstructure	Maximum shear stress (MPa)	Shear strain at maximum shear stress point (%)	Fracture shear strain (%)
Quasi-static	Unaged bimodal	655	11.4	12.2
	Over-aged bimodal	654	23.6	25.4
Dynamic	Unaged bimodal	742	8.4	15.8
	Over-aged bimodal	824	21.0	31.7

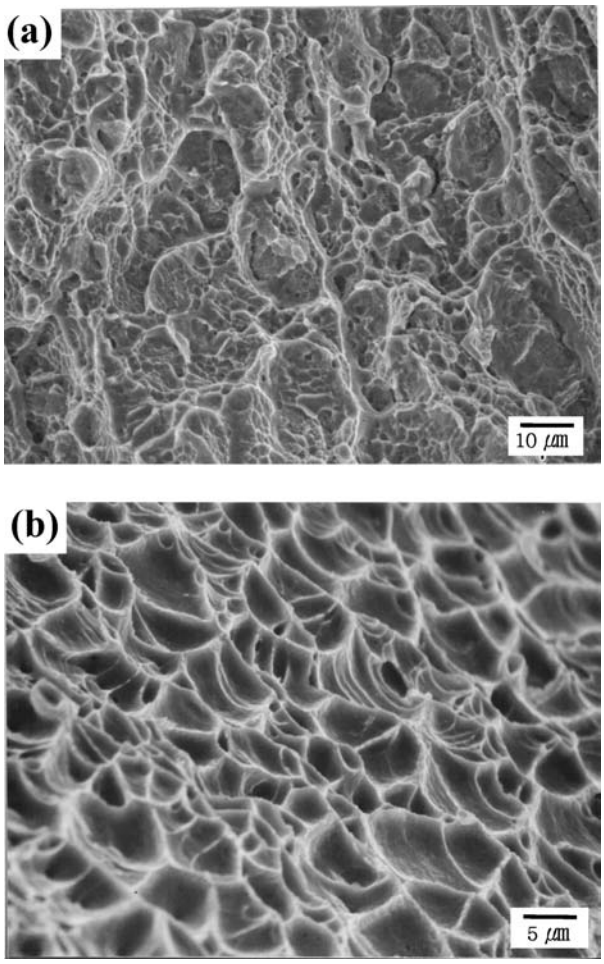

Figure 4 SEM fractographs of the tensile specimen for the (a) unaged and (b) over-aged bimodal microstructures.

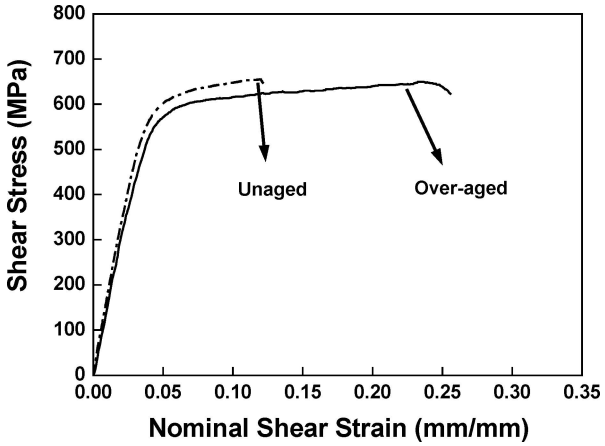

Figure 5 Shear stress-shear strain curves obtained from the quasi-static torsional test.

when compared with tensile strength. Fracture shear strain of the over-aged microstructure is twice as high as that of the unaged one, indicating that over-all quasi-static torsional properties are better in the over-aged microstructure.

Figs 6a and b are SEM micrographs of the deformed area (central area of the gage center) beneath the fracture surface of the quasi-statically fractured torsional specimens. Many voids exist at interfaces between α and tempered martensite, and the number of voids gradually decreases with increasing the depth from the

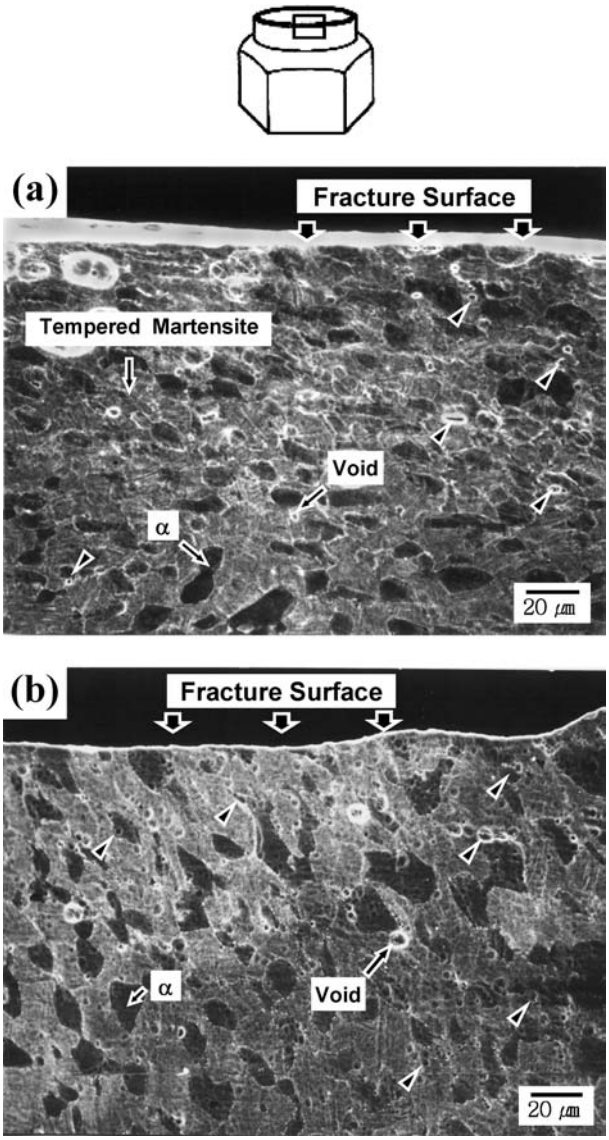

Figure 6 SEM micrographs of the deformed area (the central area of gage center) of the quasi-statically fractured torsional specimens for the (a) unaged and (b) over-aged bimodal microstructures. Kroll etched.

fracture surface. Some voids are observed even at considerable distance from the surface. The number of voids is larger in the over-aged microstructure than in the unaged microstructure (Fig. 6b).

3.4. Dynamic torsional properties

Fig. 7 shows dynamic shear stress-shear strain curves. The test data conducted under both dynamic and quasi-static loading conditions are compared in Table III. Both maximum shear stress and fracture shear strain of the over-aged microstructure are considerably higher than those of the unaged microstructure, indicating that over-all dynamic shear properties of the over-aged microstructure are improved.

SEM fractographs of dynamically fractured torsional specimens are shown in Figs 8a and b. Both the microstructures show a ductile fracture mode as in the quasi-statically fractured tensile specimens, but dimples are elongated in the shear direction. It is also observed that the dimple size of the over-aged microstructure is somewhat smaller than that of the unaged microstructure.

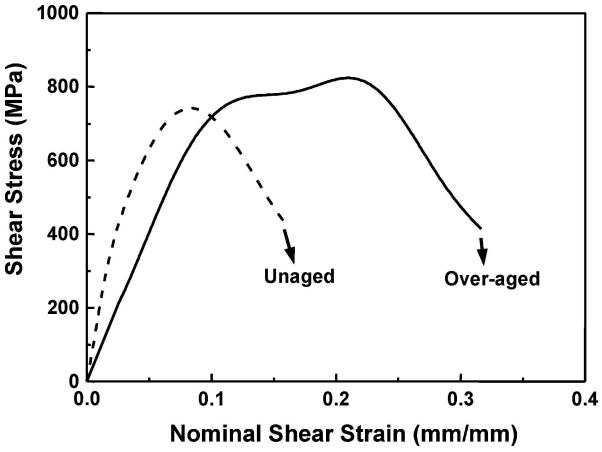

Figure 7 Shear stress-shear strain curves obtained from the dynamic torsional test.

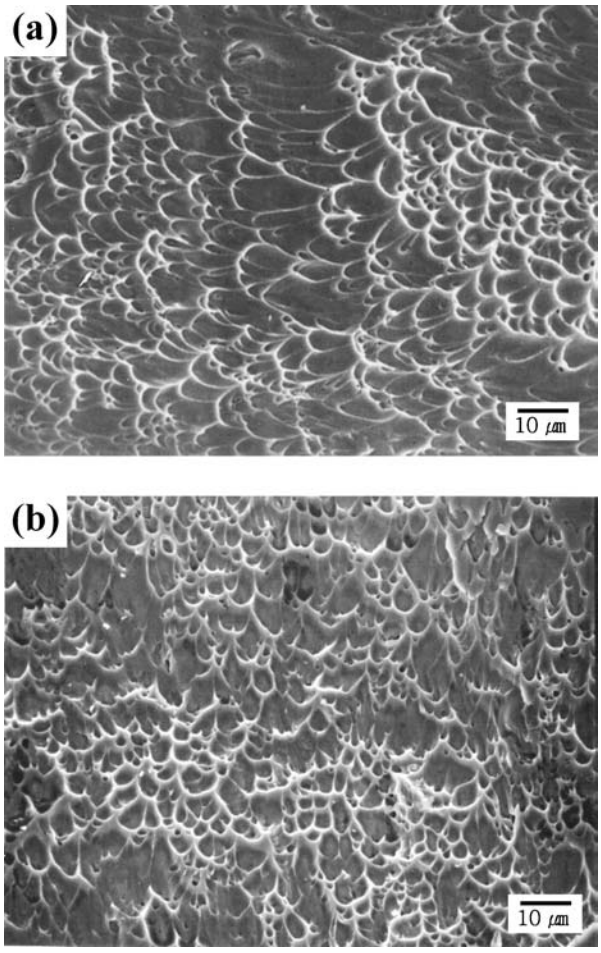

Figure 8 SEM fractographs of the dynamically fractured torsional specimens for the (a) unaged and (b) over-aged bimodal microstructures.

Figs 9a and b are SEM micrographs of the deformed area beneath the dynamically fractured surface. It is observed that voids initiate at interfaces between α and tempered martensite. The number of voids initiated near the fracture surface decreases, when compared with the quasi-static torsional test results. The number of voids is larger in the over-aged microstructure than in the unaged microstructure.

4. Discussion

Under dynamic loading, accumulated torsional waves in an extremely short period of time (several tens to

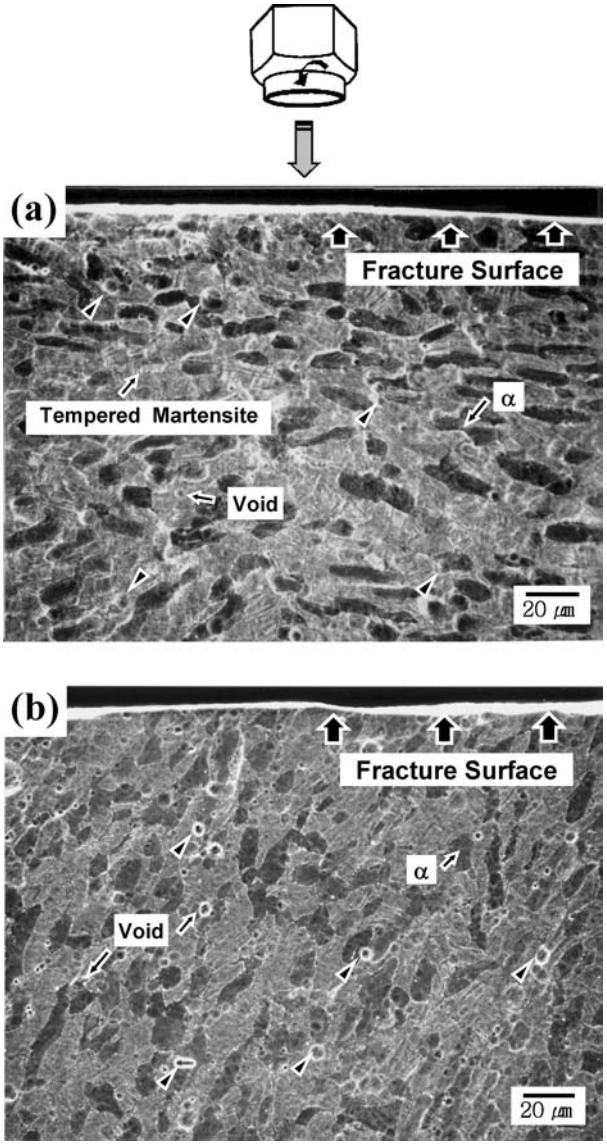

Figure 9 SEM micrographs of the deformed area (the central area of gage center) of the dynamically fractured torsional specimens for the (a) unaged and (b) over-aged bimodal microstructures. Kroll etched.

hundreds μs) are transferred to specimens to cause deformation. In Ti alloys having low heat conductivity, some local areas are in an adiabatic state because the interior heat generated from plastic deformation cannot disperse out due to insufficient time. As a result, the thermal instability increases, and plastic deformation is concentrated on the localized zone. In the areas where adiabatic shear bands are formed by localized plastic deformation, the ability to endure the load decreases abruptly, thereby leading to a rapid decrease of shear stress followed by final fracture. It is thus necessary to establish conditions to quantitatively evaluate the possibility of the adiabatic shear band formation.

Shear stress can be represented as a function of shear strain (γ), shear strain rate ($\dot{\gamma}$), and temperature (θ) as in , $\tau = f(\gamma, \dot{\gamma}, \theta)$ disregarding phenomena such as elastic deformation, strain rate, thermal history effect, and phase transformation [8, 9]. Since the maximum shear stress point is where thermal softening begins to override strain hardening and strain rate hardening, it can serve as the base point of the adiabatic shear band formation ($d\tau = 0$). According to Culver *et al.* [19],

the conditions for adiabatic shear band formation can also be expressed in terms of the heat transfer fraction of plastic deformation energy (β), density (ρ), and heat capacity (c) as follows:

$$\tau = \frac{\rho c}{\beta}\left(\frac{\partial \tau}{\partial \gamma}\right)_{\theta} \Big/ \left(-\frac{\partial \tau}{\partial \theta}\right)_{\gamma} \tag{1}$$

Equation 1 implies that maximum shear stress for adiabatic shear banding decreases, when thermal softening rate ($-\partial\tau/\partial\theta$) and heat transfer fraction (β) increase while strain hardening rate ($\partial\tau/\partial\gamma$), density ($\rho$), and heat capacity ($c$) decrease. In the actual formation of adiabatic shear bands, thermal softening sufficient to induce plastic instability should precede, although conditions satisfying equation 1 might allow the adiabatic shear band formation. It is thus required to raise the strain rate in order to provide the sufficient heat transferred from shear deformation and the adiabatic effect. The shear strain satisfying this condition can be defined as the critical shear strain (γ_c), i.e., the shear strain at the maximum shear stress point which corresponds to the point of $d\tau = 0$, on dynamic shear stress-shear strain curves. This γ_c can also be predicted from the constitutive equation which varies with plastic behavior of materials. When materials show power-law hardening behavior, the constitutive equation can be represented simply as $\tau = k\gamma^n$, where k and n are strength coefficient and strain-hardening exponent, respectively. The critical shear strain required for the adiabatic shear band formation is represented by substituting this constitutive equation to Equation 1 as below:

$$\gamma_c = n\rho c \Big/ \left(-\frac{\partial \tau}{\partial \theta}\right)_{\gamma,\dot{\gamma}} \tag{2}$$

It is learned from Equation 2 that the higher thermal softening rate ($-\partial\tau/\partial\theta$) or the less strain hardening exponent (n) could result in smaller critical shear strain (γ_c), which brings about higher possibility of the adiabatic shear band formation. From the dynamic torsional test results of Fig. 7 and Table III, the critical shear strains of the unaged and over-aged microstructures are 8.4 and 21.0%, respectively. This indicates that the over-aged microstructure is less vulnerable to shear localization and thus to adiabatic shear band formation than the unaged microstructure.

In general, dynamic torsional deformation of ductile metals develops in the following three stages [17, 20–22]: (1) homogeneous deformation stage before reaching maximum shear stress, (2) inhomogeneous deformation stage starting from maximum shear stress point, and (3) stage of initiation and development of adiabatic shear bands due to shear localization. In the last stage, a radical temperature rise accompanies the adiabatic shear band formation. Considering the adiabatic shear band formation as a result of the plastic instability combined with the local temperature rise, the maximum shear stress where the inhomogeneous stage commences can be considered to be the starting point of the adiabatic shear band initiation. The area below the dynamic shear stress-shear strain curve of Fig. 7 from the origin to the maximum shear stress point indicates the absorbed energy per unit volume as the material deforms until the adiabatic shear band initiates. This absorbed energy, E_c, can be formulated as below:

$$E_c = \int_0^{\gamma_{\max}\ at\ \tau_{\max}} \tau d\gamma \tag{3}$$

Assuming a considerable amount of energy produced during dynamic torsional deformation is absorbed by plastic shear deformation, the larger is the value of E_c, the more difficult is the adiabatic shear band formed. The curve after the maximum shear stress point does not have any implications in evaluating the adiabatic shear band formation since the material loses the load-carrying ability at the commencement of the adiabatic shear band formation [9, 23]. The E_c values calculated from the dynamic shear stress-shear strain curves of Fig. 7 are 45.5×10^6 and 125×10^6 J/m^3, respectively, for the unaged and over-aged microstructures. This implies that the energy required for forming adiabatic shear bands during dynamic deformation is greater in the over-aged microstructure than in the unaged microstructure, thereby lowering the possibility of the adiabatic shear band formation in the over-aged microstructure.

This deformation energy also works as driving force for ductile fracture through void initiation, growth, and coalescence, and is partly used for the adiabatic shear banding. When the deformation energy is introduced into the specimen interior, it is transformed to thermal energy and stored in some areas [24–27]. When part of it is used for void initiation under dynamic loading, the deformation energy required for the adiabatic shear band formation is thus reduced as much. In order to quantitatively interpret the possibility of the adiabatic shear band formation, the number of voids per unit area in the deformed region beneath the fracture surface was measured, and the results are shown in Fig. 10. In the over-aged microstructure, the number of voids is 2.5 times greater than that in unaged microstructure. Figs 9a and b confirm that the void initiation is more

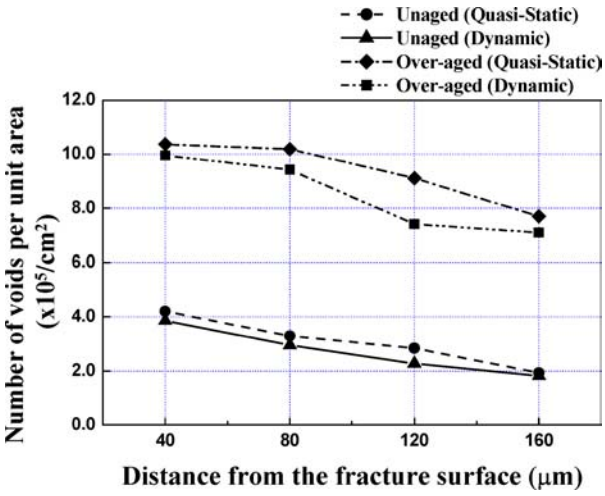

Figure 10 Number of voids per unit area as a function of distance from the fracture surface for the unaged and over-aged bimodal microstructures.

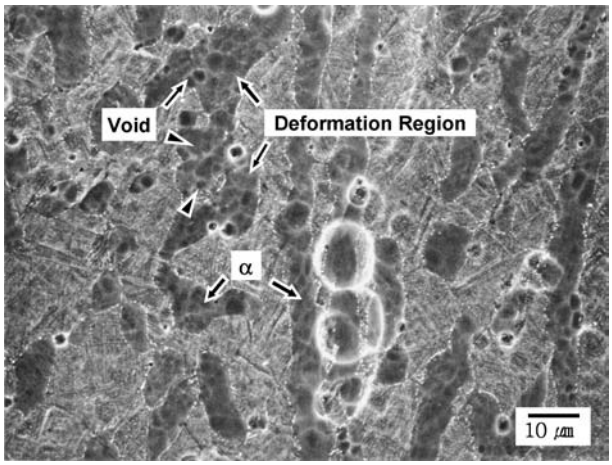

Figure 11 High-magnification SEM micrograph of the deformed area of the dynamically fractured torsional specimen for the over-aged bimodal microstructure, showing many voids located inside α phases. Kroll etched.

frequently observed in the deformed area of the over-aged microstructure due to the precipitation effect of α_2 phases. In a higher-magnification SEM micrograph (Fig. 11) of the deformed area, many voids are observed inside α phases as well as at interfaces between α and tempered martensite. It is also noted that dimple sizes in tensile and torsional specimens of the over-aged microstructure are smaller than those of the unaged microstructure (Figs 8a and b). This implies that α_2 particles can work as void initiation sites, although they are very fine. Since the number of voids formed in the over-aged microstructure drastically increases because of the α_2 precipitation, driving force for the adiabatic shear band formation decreases as much as deformation energy used for the void formation, reducing the possibility of the adiabatic shear band formation. These results match well with the aforementioned results of γ_c and E_c, and thus it is confirmed again that the possibility of the adiabatic shear band formation is lower in the over-aged microstructure than in the unaged microstructure.

The precipitation of very fine α_2 particles through over-aging of the bimodal microstructure increases dynamic torsional properties as well as quasi-static properties. It also reduces the possibility of the adiabatic shear band formation, and thus suggests a new approach to improve ballistic performance and to find optimal process conditions in high-speed metal forming.

5. Conclusions

The quasi-static and dynamic torsional deformation behavior of the bimodal microstructure containing fine α_2 particles was investigated, and the results were analyzed in relation to critical shear strain, absorbed deformation energy, void initiation, and adiabatic shear banding.

(1) In the over-aged bimodal microstructure, fine α_2 particles of 50–200 nm in size were homogeneously distributed in α phases. The quasi-static torsional test data indicated that the over-aged microstructure showed higher fracture shear strain than the unaged microstructure, while their maximum shear stress was similar. Voids were initiated mainly at interfaces between α and tempered martensite.

(2) Under dynamic torsional loading, maximum shear stress and maximum shear strain of the over-aged microstructure were higher than those of the unaged microstructure. The number of voids was larger in the over-aged microstructure than in the unaged microstructure because of the additional precipitation effect of α_2 phases.

(3) The possibility of the adiabatic shear band formation under dynamic loading was quantitatively analyzed by introducing concepts of critical shear strain, absorbed deformation energy, and void initiation. In the over-aged microstructure, the energy required for forming adiabatic shear bands was greater than in the unaged microstructure, thereby lowering the possibility of the adiabatic shear band formation.

(4) The precipitation of very fine α_2 phases through over-aging of the bimodal microstructure improved dynamic torsional properties as well as quasi-static properties, and reduced the possibility of adiabatic shear banding, thereby suggesting a new approach to improve ballistic performance of Ti alloy armor plates.

Acknowledgments

This work was supported by the National Research Laboratory Program funded by the Ministry of Science and Technology, Korea. The authors thank Professor Chong Soo Lee and Mr. Youwhan Lee of POSTECH for their help on the heat-treatment of the Ti-6Al-4V alloy.

References

1. D. EYLON, J. A. HALL, C. M. PIERCE and D. L. RUCKEL, *Metall. Trans.* A **7A** (1976) 1817.
2. M. HAGIWARA, S. EMURA, A. ARAOKA, B. O. KONG and F. TANG, *Met. Mater. Intern.* **9** (2003) 265.
3. G. THOMAS, V. RAMACHANDRA, K. V. NAGARAJAN, B. PANT, B. K. SARKAR and R. VASUDEVAN, *Welding Res. Suppl.* **8** (1989) 336.
4. A. GYSLER and G. LUTJERING, *Metall. Trans.* A **13A** (1982) 1435.
5. S. L. SEMIATIN and T. R. BIELER, *Metall. Mater. Trans.* A **32A** (2001) 1871.
6. K. SUZUKI and M. YAO, *Met. Mater. Intern.* **10** (2004) 33.
7. A. CHO, R. F. ASHTON, G. W. STEELE and J. L. KIRBY, in Proc. 5th Int. Conf. of Aluminum-Lithium Alloys, edited by T. H. Sanders, Jr. and E.A. Starke, Jr. (Material and Composite Engineering Publication Ltd., Birmingham, UK, 1989) vol. III, p. 1377.
8. M. A. MEYERS, "Dynamic Behavior of Materials" (John Wiley & Sons, NY, 1994) p. 448.
9. Y. BAI and B. DODD, "Adiabatic Shear Localization-Occurrence, Theories and Applications" (Pergamon Press, NY, 1992) p. 125.
10. S. LEE, K. CHO, K. J. KIM and W. B. CHOI, *Metall. Trans.* A **24A** (1993) 895.
11. D.-G. LEE, S. KIM, S. LEE and C. LEE, *Metall. Mater. Trans.* A **32A** (2001) 315.
12. G. WELSCH, G. LUETJERING, K. GAZIOGLU and W. BUNK, *Metall. Trans.* **8A** (1977) 169.
13. H. MARGOLIN, J. C. WILLIAMS, J. C. CHESNUTT and G. LUETJERING, in Proc. of the 4th Int. Conf. on Ti (Koyto, Japan, 1980) vol. 1, p. 169.
14. *Idem.*, in Proc. of the 4th Int. Conf. on Ti (Koyto, Japan, 1980) vol. 1, p. 277.

15. R. BOYER, G. WELSCH and E. W. COLLINGS, in "Materials Properties Handbook: Titanium Alloys" (ASM, Materials Park, OH, 1994) p. 491.
16. "Metals Hand Book" (9th ed., ASM, Metals Park, OH, 1990) vol. 8, p. 218.
17. A. MARCHAND and J. DUFFY, *J. Mech. Phys. Solids* **36** (1988) 251.
18. S. KIM and S. LEE, *Metall. Mater. Trans.* A **31A** (2000) 1753.
19. R. S. CULVER, "Metallurgical Effects at High Strain Rates" (Plenum Press, NY, 1973) p. 519.
20. K. CHO, Y. C. CHI and J. DUFFY, *Metall. Trans.* A **21A** (1990) 1161.
21. K. CHO, S. LEE, S. R. NUTT and J. DUFFY, *Acta Metall.* **41** (1993) 923.
22. W. S. SHIM and D. B. LEE, *Met. Mater. Intern.* **9** (2003) 473.
23. C. G. LEE, W. J. PARK, S. LEE and K. S. SHIN, *Metall. Trans.* A **29A** (1998) 477.
24. J. WADSWORTH, I. G. PLAMER and D. D. CROOKS, *Scripta Metall.* **17** (1983) 347.
25. H. Y. KIM, J. MATSUDA and K. MARUYAMA, *Met. Mater. Intern.* **9** (2003) 255.
26. M. A. MEYERS and C. L. WITTMAN, *Metall. Trans.* A **21A** (1990) 3153.
27. C. L. WITTMAN, M. A. MEYERS and H.-R. PAK, *Metall. Trans.* A **21A** (1990) 707.

Received 1 October 2003
and accepted 11 March 2005